HyPyRameter: A Python Toolbox to Calculate Spectral Parameters from Hyperspectral Reflectance Data

Michael S. Phillips[1], Christian Tai Udovicic[2] [iD], Jeffrey E. Moersch[3], Udit Basu[3], and Christopher W. Hamilton[1] [iD]
[1] Lunar and Planetary Laboratory, The University of Arizona, Tucson, AZ, USA
[2] Hawaii Institute of Geophysics and Planetology, The University of Hawaii at Manoa, Manoa, HI, USA
[3] Department of Earth and Planetary Sciences, The University of Tennessee, Knoxville, TN, USA

Abstract

Hyperspectral image cubes are information rich, typically containing hundreds of wavelengths and millions of spatial pixels. To condense this information into a more interpretable form, it is common to parameterize certain aspects of the spectra that are known to represent compositions of interest. Parameterizations of spectral features are called *spectral parameters*. Spectral parameters can be combined thematically into red, green, and blue (RGB) images, called *browse products*, to visualize compositional variation across a surface. Here, we present the Hyperspectral Parameter (HyPyRameter) toolbox: an open-source library, written in Python, to calculate spectral parameters for hyperspectral reflectance data. With the HyPyRameter toolbox, a user can calculate spectral parameters from point spectra or hyperspectral image cubes. Users can take advantage of the native parameters built into the HyPyRameter library, or easily customize the library of parameter formulas with built-in functions to suit the needs of a specific investigation. HyPyRameter can be run with Jupyter notebooks provided on the GitHub repo (https://github.com/Michael-S-Phillips/HyPyRameter). HyPyRameter is a flexible tool, installable via Anaconda (https://anaconda.org/michael–s–phillips/hypyrameter), with potential for wide-ranging applications to diverse fields including, but not limited to, planetary science, geology, agriculture, and mineral resource exploration.

Unified Astronomy Thesaurus concepts: Spectroscopy (1558); Surface composition (2115)

1. Introduction

Many materials, including Fe-bearing silicates, phyllosilicates, amorphous silica phases, carbonates, sulfates, and oxides, display diagnostic absorption features in visible to short-wavelength infrared (VSWIR; ~400–4000 nm) reflectance spectra (J. B. Adams & A. L. Filice 1967; R. N. Clark et al. 1990; R. G. Burns 1993). Thus, reflectance spectrometers are excellent tools for mapping terrestrial and planetary surface compositions (J. B. Adams 1974). Field applications of reflectance spectroscopy on Earth typically use handheld point spectrometers or specialized aircraft-mounted imaging spectrometers, such as the Airborne Visible InfraRed Imaging Spectrometer (S. A. Macenka & M. P. Chrisp 1987). However, field-deployable hyperspectral push-broom imagers capable of collecting data at the outcrop-scale (B. Van Gorp et al. 2014; J. Moersch et al. 2020) and landscape-scale from a motorized tripod-mounted platform or a nadir-pointing drone-mounted platform (J. Moersch et al. 2020) are expanding the potential for field applications of hyperspectral reflectance spectroscopy (U. Basu et al. 2023; N. T. Stein et al. 2023).

Hyperspectral image cubes contain an immense amount of information, which can make finding the most meaningful aspects of the data a labor-intensive task. One data-processing solution is to parameterize characteristics of a spectrum (R. N. Clark & T. L. Roush 1984; S. M. Pelkey et al. 2007; C. E. Viviano et al. 2014). "*Spectral parameters*" can be formulated for specific absorption bands and other features

associated with compositions of interest to quickly identify regions of interest across a scene for further spectral analysis.

The calculation of spectral parameters carries certain advantages over other hyperspectral data reduction and analysis methods. Eigenanalysis-based methods, such as principal component analysis, minimum noise fraction transformations, and independent component analysis, are used to reduce spectral dimensionality and retrieve the components responsible for the most in-scene spectral variance. These tools can be used to find in-scene spectral endmembers, classify these spectral endmembers with reference to library data, generate spectral-endmember unit maps, and calculate relative contributions of each spectral endmember to every pixel. While a useful and powerful tool, such data reduction methods are inherently scene-dependent making cross-scene comparisons difficult, and require expert knowledge to generate, interpret and communicate. Additionally, such methods cannot work on smaller data sets, such as an individual spectrum. Another common method for spectral data analysis is to compare every spectrum in a scene to a library of reference spectra and label each pixel with the closest-fit reference spectrum (e.g., Tetracorder, R. N. Clark et al. 2003). The advantage of a tool such as Tetracorder is that pixels are identified as a specific mineral; however, these classifications are inherently limited by the makeup of the reference spectral library and are vulnerable to natural differences in spectral shape that may occur between in-scene and reference spectra. Calculation of spectral parameters has the advantage of enabling cross-scene comparison, functioning on a single spectrum, and ease of interpretation by a nonexpert. However, parameters must be defined a priori, with the risk of missing unusual compositions not captured with a given set of parameters. Therefore, it can be advantageous to employ a diverse set of data analysis methods. HyPyRameter facilitates
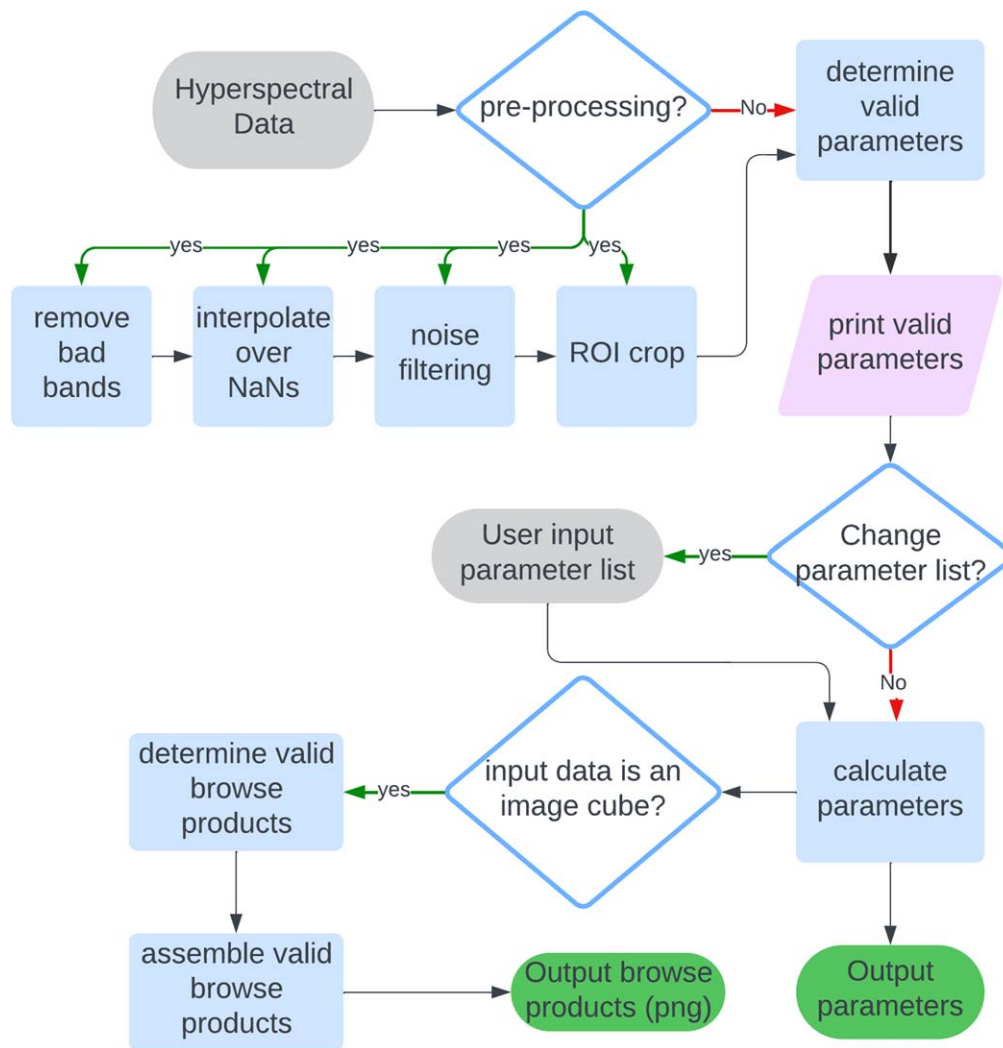
Figure 1. Flowchart delineating the HyPyRameter protocol. The user inputs hyperspectral data (either an image cube or point spectra), with optional preprocessing. Valid parameters are determined based on the wavelength range of the data and printed for user evaluation. Users can further cull the list of valid parameters or run all parameters in the list. Parameters are calculated and returned as an image cube or series of vectors depending on input data type. If input data is an image cube, browse products are also calculated and returned.

the inclusion of spectral parameterization into the remote sensing scientists' toolkit.

2. Contents of the HyPyRameter Toolbox

The HyPyRameter toolbox allows users to calculate spectral parameters on VSWIR hyperspectral reflectance data. The term "hyperspectral" means that spectral sampling is contiguous and that spectral features are oversampled by the data. Image cubes must be in ENVI format, that is a disk image (.img) file with an associated header file (.hdr), and point spectra can be formatted as .sed, csv, excel, or a pandas data frame. Any hyperspectral VSWIR data, formatted as described above, can be used with HyPyRameter (Figure 1). The toolbox includes formulations for reflectance, band depth, inverted band depth (aka band height), N-band minimum (MIN), shoulder drop-off, shoulder height, spectral index, normalized difference indices, and reflectance peak calculations. Below we describe each type of spectral parameter implemented in HyPyRameter. Figure 2 illustrates the implementation of four of the basic parameters.
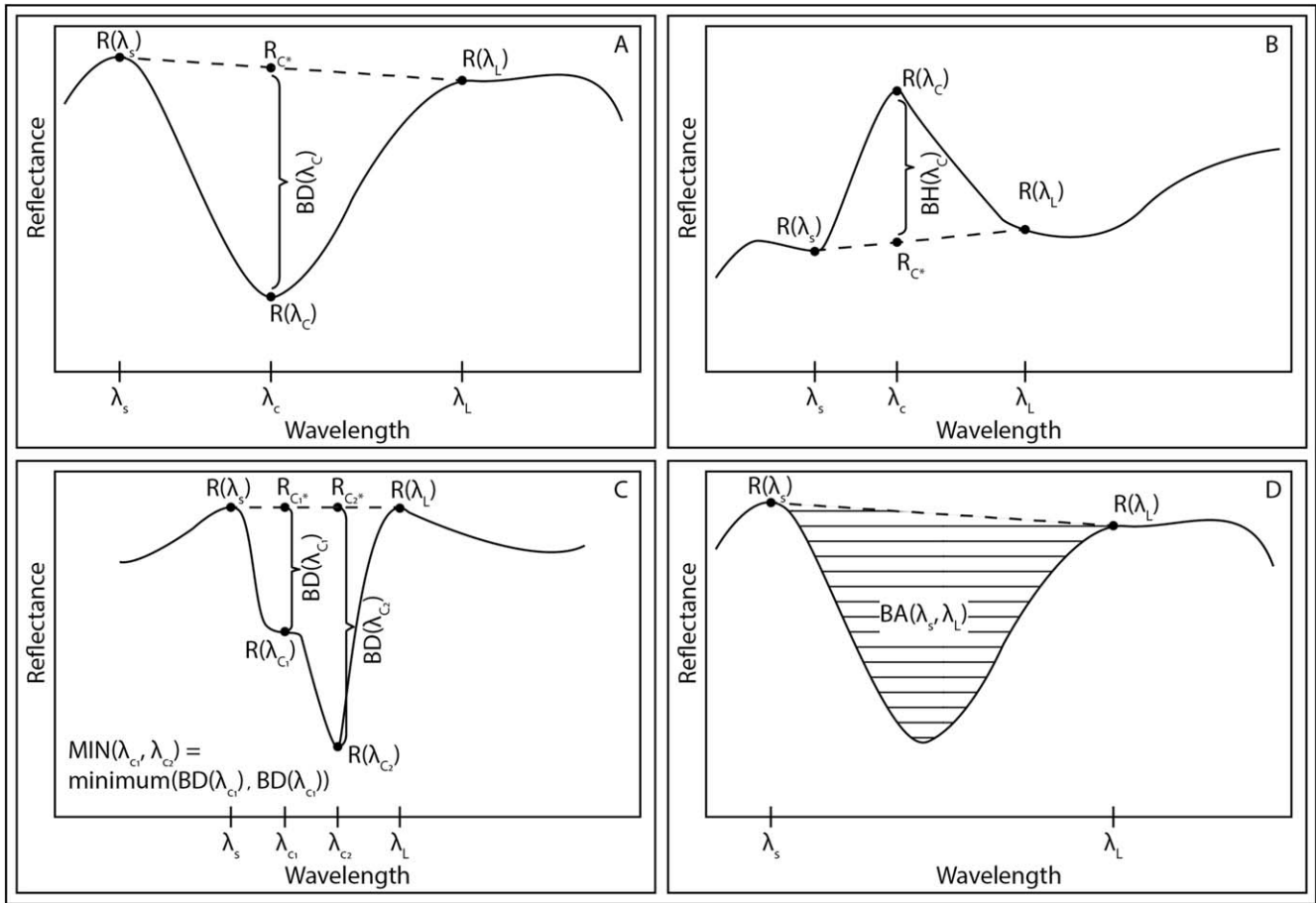
2.1. Parameters

2.1.1. Reflectance

The reflectance (R) band parameter simply returns the reflectance value of the hyperspectral cube at the wavelength nearest the requested wavelength (λ). For example, $R(\lambda)$ is calculated by subtracting λ from the wavelength vector, retrieving the index of the minimum absolute value (m_i), then returning the reflectance value at m_i. Reflectance parameters can be used to construct approximate true color images from the data, "enhanced color" images using nonvisible wavelengths, and return reflectance values used in other parameter calculations. The default option for R parameters is to return the median filtered reflectance value with a kernel width of 5 spectral channels.

2.1.2. Band Depth

Band depth (BD) calculations are among the most common spectral parameters used for analysis of hyperspectral data (e.g., R. N. Clark & T. L. Roush 1984). For HyPyRameter, we have adopted the BD formulation (Equation (1)) from C. E. Viviano et al. (2014), wherein the BD is equal to one

Figure 2. Illustration of four basic parameters in the HyPyRameter library. (A) Band depth parameter, (B) Band height parameter, (C) MIN parameter, and (D) Band Area.

minus the ratio of the reflectance value at a central wavelength (λ_c) to an interpolated continuum value at that same wavelength (R_{c*}):

$$\mathrm{BD}(\lambda_c) = 1 - \frac{R(\lambda_c)}{R_{c^*}} \quad (1)$$

$$R_{c^*} = bR(\lambda_s) + aR(\lambda_l) \quad (2)$$

$$a = \frac{\lambda_c - \lambda_s}{\lambda_l - \lambda_s}; \; b = 1 - a. \quad (3)$$

The continuum reflectance value (R_{c*}, Equation (2)) is calculated via weighted linear interpolation from nearby shorter (λ_s) and longer (λ_l) wavelengths using the weighting parameters a and b (Equation (3)). The parameters λ_s and λ_l are free parameters chosen for each band parameter (Table A1).

2.1.3. Inverted Band Depth (Band Height)

The Inverted Band Depth parameter, or Band Height (BH), calculates the height of a feature above an interpolated continuum value. The BH parameter is formulated as follows (C. E. Viviano et al. 2014):

$$\mathrm{BH}(\lambda_c) = 1 - \frac{R_{c^*}}{R(\lambda_c)}. \quad (4)$$

2.1.4. N-band Minimum (MIN)

The *N*-band Minimum, or MIN, spectral parameter is useful for quantifying spectral features composed of multiple,

partially overlapping absorption features, such as the kaolinite doublet or the gypsum triplet features. The MIN parameter formulation employed in HyPyRameter is modified after C. E. Viviano et al. (2014) and is calculated as follows:

$$\mathrm{MIN}(\lambda_1 , ... \, \lambda_n) = \mathrm{minimum}(\mathrm{BD}(\lambda_1) , ... \, \mathrm{BD}(\lambda_n)). \quad (5)$$

The minimum function carries certain advantages over a geometric mean, such as higher sensitivity to cases in which both absorption features in the doublet are strongly absorbing and robustness against false positive values in the case of inverted features (see C. E. Viviano et al. 2014 for more details).

2.1.5. Shoulder Drop-off and Shoulder Height

Some absorption features appear as a steep drop-off in reflectance with no symmetric rise. Such features are referred to as "shoulders." The Shoulder Drop-off (*D*) parameter captures the depth of the base of a shoulder feature relative to its peak. The interpolated continuum for calculation of a *D* parameter is formulated to extend over the top of a shoulder feature. Example formulations of *D* can be found in Table A1.

Shoulder Height (SH) parameters are analogous to BH parameters but for shoulder features rather than symmetric reflectance peaks. Calculation of SH parameters interpolate a continuum beneath the shoulder feature and calculate the height to the peak of the shoulder from the interpolated continuum (see Table A1 for example formulations).

2.1.6. Spectral Index Parameters

Some minerals, such as olivine, pyroxene, and sulfates, have multiple absorption bands that create broad-band, composite features. The spectral signature of olivine comprises three Gaussian-shaped crystal-field absorptions that overlap to create a broad absorption feature centered around 1 μm. Pyroxenes show two broad-band absorption features centered around approximately 1 and 2 μm. Mono- and polyhydrated sulfates absorb at approximately 2.1 and 2.4 μm, creating a convex-up feature between these two absorptions. Pigments, such as chlorophyll, can also show a composite feature in the visible to near-infrared wavelength region due to multiple types of chlorophyll and chlorophyll-related protein complexes. Spectral features composed of multiple absorptions can be parameterized, and such parameters are called an *Index*. Index parameter formulations are typically unique to a mineral, or mineral group, of interest. In general, parameters are not sensitive to specific minerals but can be sensitive to mineral groups (e.g., carbonates, smectites, pyroxenes, etc.). Examples of Index parameters are listed in Table A1.

2.1.7. Normalized Difference Indices

The HyPyRameter toolbox includes normalized difference indices (NDI), calculated as:

$$\text{NDI}(a, b) = (a - b)/(a + b), \quad (6)$$

where a and b are the reflectance value at a given wavelength. The three NDIs included in HyPyRameter are the normalized difference vegetation index (NDVI), moisture index (NDMI), and water index (NDWI). The NDVI, NDMI, and NDWI use $(a, b) = (R(665\,\text{nm}), R(833\,\text{nm}))$, $(R(833\,\text{nm}), R(1670\,\text{nm}))$, and $(R(560\,\text{nm}), R(833\,\text{nm}))$, respectively, taken after the wavelengths used for calculation of these indices by Sentinel.[4]

2.1.8. Other Parameters

Additional parameters included in the HyPyRameter toolbox include peak reflectance (RPEAK), integrated band depths (BDI), band areas (BA), band ratios (BR), and slopes (SLOPE). RPEAK parameters fit a polynomial to a spectral region of interest and return both the wavelength and reflectance value of the reflectance peak over that spectral region; for example, in the case of RPEAK1, a fifth-order polynomial is fit to reflectance values between 442 and 989 nm. BDI parameters return the integral of a polynomial fit to a spectral region of interest normalized to the peak reflectance value over that region. Band area (BA) parameters return the continuum subtracted area between two wavelength values. The band area is calculated via integration of a cubic spline fit to the spectrum between the chosen wavelengths. As their names imply, BR parameters calculate the ratio of reflectance values at two wavelengths, and SLOPE parameters return the slope between two values returned in units of reflectance/μm. For an assessment of the effect of noise on parameter calculations, see Figure A1.

2.2. Utilities

The HyPyRameter tool includes several options for cleaning spectral data before calculation of spectral parameters. Users

---

Table 1
Browse Products Natively Available in HyPyRameter Param1, Param2, and Param3 Correspond to the Red, Green, and Blue Image Channels, Respectively

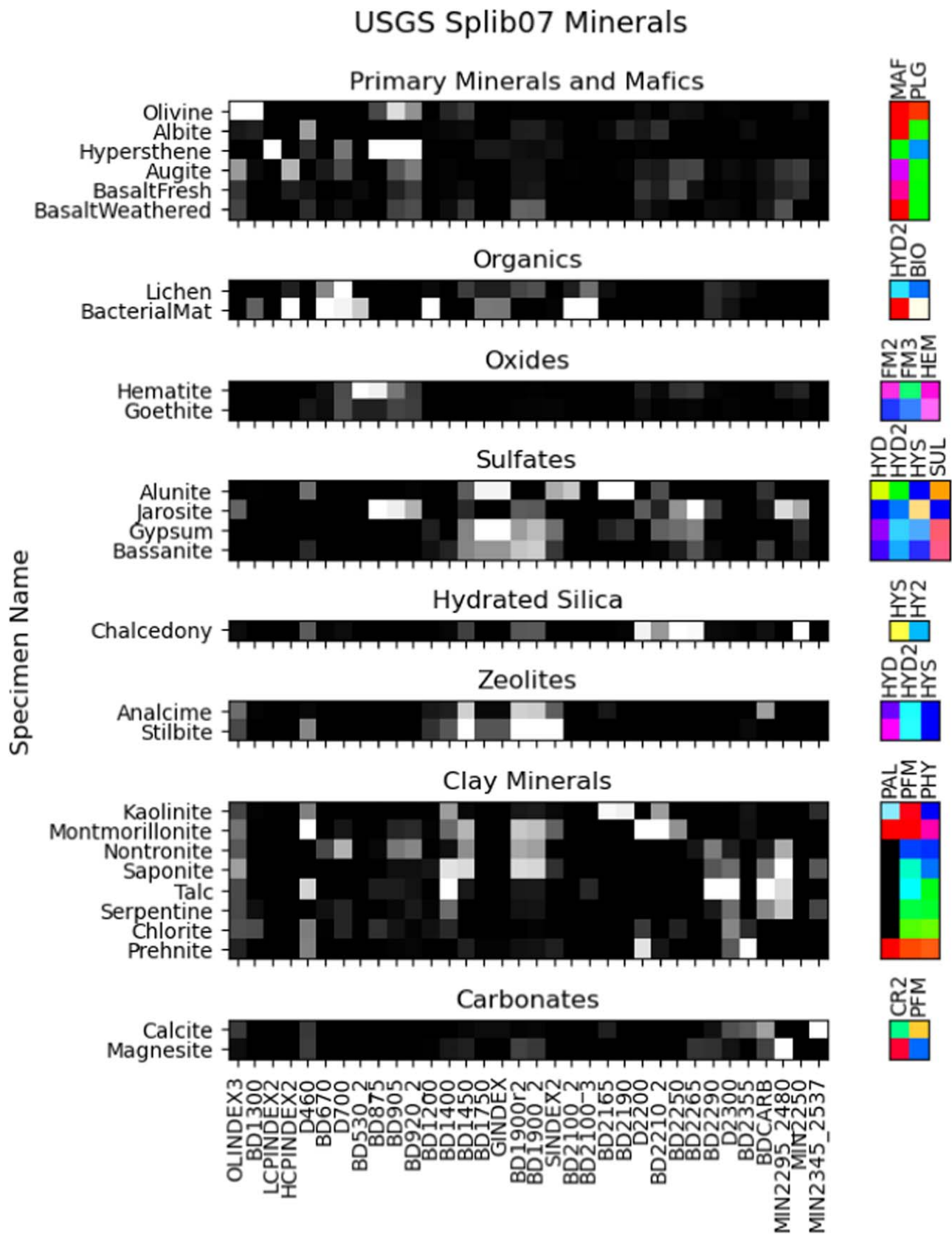| Browse Product	Param1	Param2	Param3
BIO	CPLINDEX	NDVI	D700
CR2	MIN2295_2480	MIN2345_2537	BDCARB
FAL	R2529	R1506	R1080
FM2	BD530_2	BD920_2	BDI1000VIS
FM3	BD670	BD875	BD905
HEM	BD530_2	BD670	BD875
HYD	SINDEX2	BD2100_2	BD1900_2
HYD2	BD1200	BD1450	BD1900r2
HYD3	BA1200	BA1450	BA1900
HYS	MIN2250	BD2250	BD1900r2
MAF	OLINDEX3	LCPINDEX2	HCPINDEX2
PAL	BD2210_2	BD2190	BD2165
PFM	BD2355	D2300	BD2290
PHY	D2200	D2300	BD1900r2
PLG	BD1300	RPEAK1	LCPINDEX2
SED	BDCARB	BD2100_3	GINDEX
SUL	GINDEX	SINDEX2	BD2265
TRU	R637	R550	R463

can include a list of bad bands, interpolate across bad data values determined by the bad bands list, and run a spectral denoising routine. A simple linear interpolation is used to interpolate over bad bands, but this routine can yield more accurate results for certain BD calculations, specifically over regions where atmospheric absorptions affect the spectrum. The noise filtering routine employed by HyPyRameter is a generalized version of the Iterative Outlier Voting Filter (IOVF) from M. S. Phillips et al. (2023b). This routine calculates outlier statistics through convolution of a $7 \times 5 \times 5$ kernel (row, column, band) with the image cube to identify outlier pixels. Outlier pixels are updated through an exponential distance weighted interpolation of neighboring spatial and spectral pixel values. The IOVF routine is more appropriate for hyperspectral than multispectral data because it uses information from adjacent spectral channels to calculate outlier statistics and update bad pixel values. More details on the IOVF routine can be found in M. S. Phillips et al. (2023b).
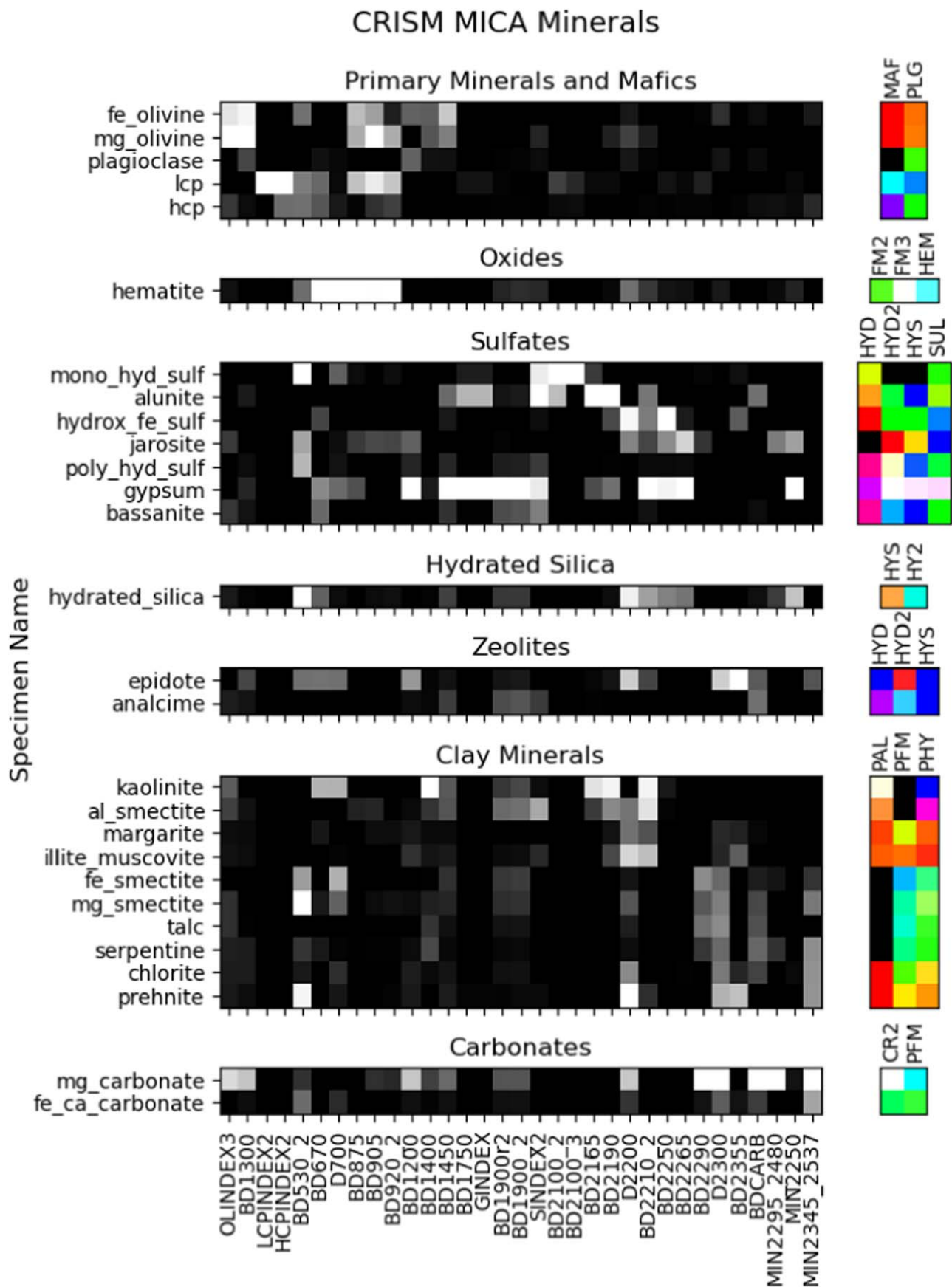
2.3. Browse Products

Spectral parameter calculations return a grayscale image that is bright where a spectral feature is present and dark where it is not—a form of the data that is readily interpretable. Thematically related spectral parameter images can be combined into three-band color "*browse products*" in which color variations indicate changes and mixtures of compositions across the scene. Standard spectral parameter combinations (C. E. Viviano et al. 2014) have been established for visualizing Compact Reconnaissance Imaging Spectrometer for Mars (CRISM; S. Murchie et al. 2007) data, and we have included a number of these standard browse product

Figure 3. Application of HyPyRameter to select minerals from the USGS SpecLib v7. Parameter values are represented as "single pixels" (black = low values, white = high values). Expected colors for browse product combinations are shown along the right side.

Figure 4. Application of HyPyRameter to the CRISM MICA library. Parameter values are represented as "single pixels" (black = low values, white = high values). Expected colors for browse product combinations are shown along the right side.

RAVEN Specimens and USGS Splib07 Minerals
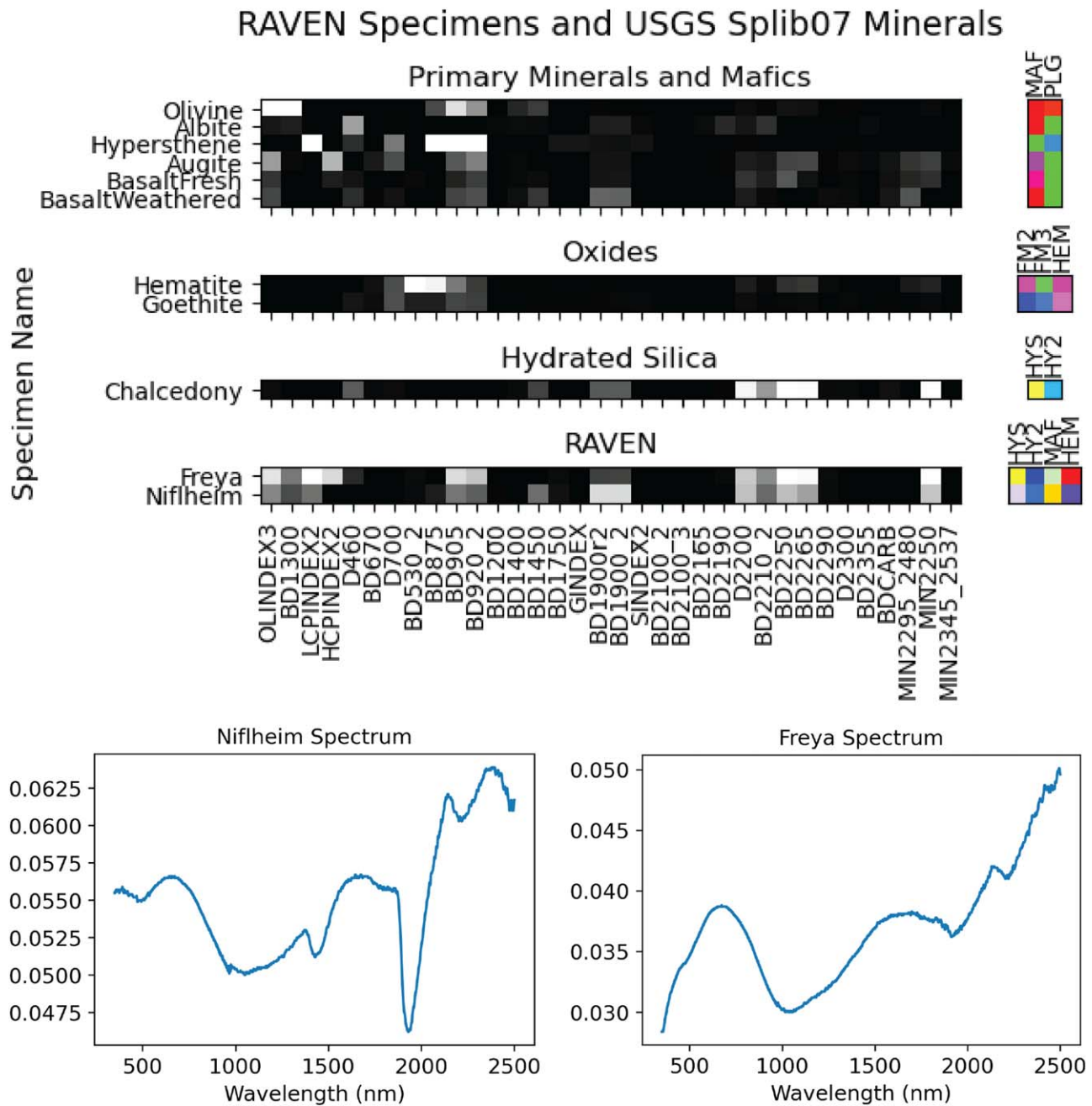
Figure 5. HyPyRameter results on point spectra from samples collected for the Rover–Aerial Vehicle Exploration Network (RAVEN) project. Parameter values for the Freya and Niflheim RAVEN samples are represented as "single pixels" and compared with USGS library spectra for reference. Pyroxene is indicated by high LCPINDEX2, BD905, and BD920_2 values, and H_2O bonds are indicated by high BD1900r2 and BD1900_2 values. Small amounts of iron oxides are indicated in both spectra by purple/red color values in the HEM browse product, and hydrated silica is indicated by high D2200, BD2250, and BD2265 values combined with high BD1900_2 values.

combinations with HyPyRameter, as well as several new combinations applicable to Earth-based data (see Table 1). For example, the "BIO" browse product includes three parameters sensitive to the presence of chlorophyll: the CPLINDEX, NDVI, and D700 parameters.

3. Example HyPyRameter Output

Below we show sample HyPyRameter output across a range of data sets, including results from the Rover–Aerial Vehicle Exploration Network (RAVEN) campaign in Iceland (Carr et al. 2024; S. Gwizd et al. 2024; C. W. Hamilton et al.

2024), a mission simulation in a planetary analog terrain. We demonstrate results from HyPyRameter on point spectra and spectral image cubes collected via tripod-, drone-, and orbital-based platforms for Earth and Mars.

3.1. Reference Spectral Libraries

We first show parameter values calculated on spectra from the United States Geological Survey (USGS) Spectral Library (R. Kokaly et al. 2017) and the Minerals Identified through CRISM Analysis (MICA) Library (C. E. Viviano et al. 2014) to demonstrate spectral parameter response to reference
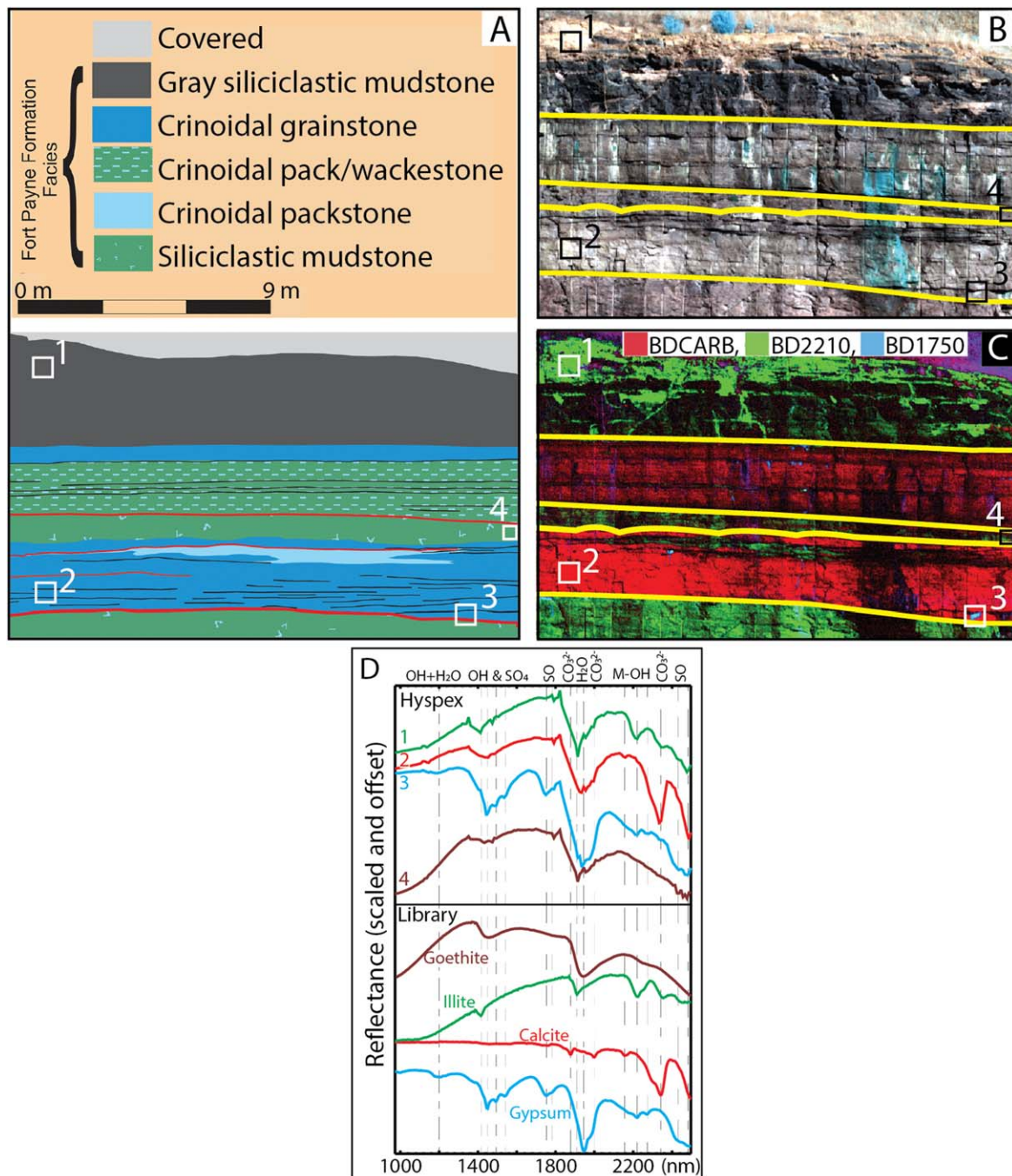
Figure 6. Application of HyPyRameter to a roadcut along TN52, Tennessee. The formation facies (A) containing (hydrated) carbonates (calcite) and clays (illite) are readily distinguishable using spectral parameters (C). Panel (B) shows the outcrop with an FAL browse product (R2529, R1506, R1080). Panel (D) shows representative spectra from the locations indicated in panels (A)–(C).

compositions (Figures 3, 4). Parameter values are displayed as "single pixels," where the brightness value correlates positively with the parameter value. Relevant browse product combinations were calculated for each reference mineral spectrum to demonstrate idealized color responses that these compositions will have in those browse product combinations.

3.2. Point Spectra from the Icelandic Highlands

The RAVEN campaign in Iceland was the motivating factor for the development of HyPyRameter. VSWIR data were collected to support both rover and Unoccupied Aircraft System (UAS, or drone) mission simulation activities at the Holuhraun eruption site (G. B. M. Pedersen et al. 2017; J. R. C. Voigt et al. 2021), and reduced data products were desired to facilitate interpretation by the Science Operations Teams (Carr et al. 2024, in press; S. Gwizd et al. 2024). Figure 5 shows example spectra collected in the field in support of the RAVEN mission simulation, and associated HyPyRameter output represented as single pixel brightness values as in Figures 3 and 4. HyPyRameter results indicate that one sample collected during the mission campaign, Freya, is consistent with olivine, low-calcium pyroxene, hydrated silica, and hematite, whereas another sample, Niflheim, is consistent with olivine, hydrated silica, and to a lesser extent pyroxene and hematite.
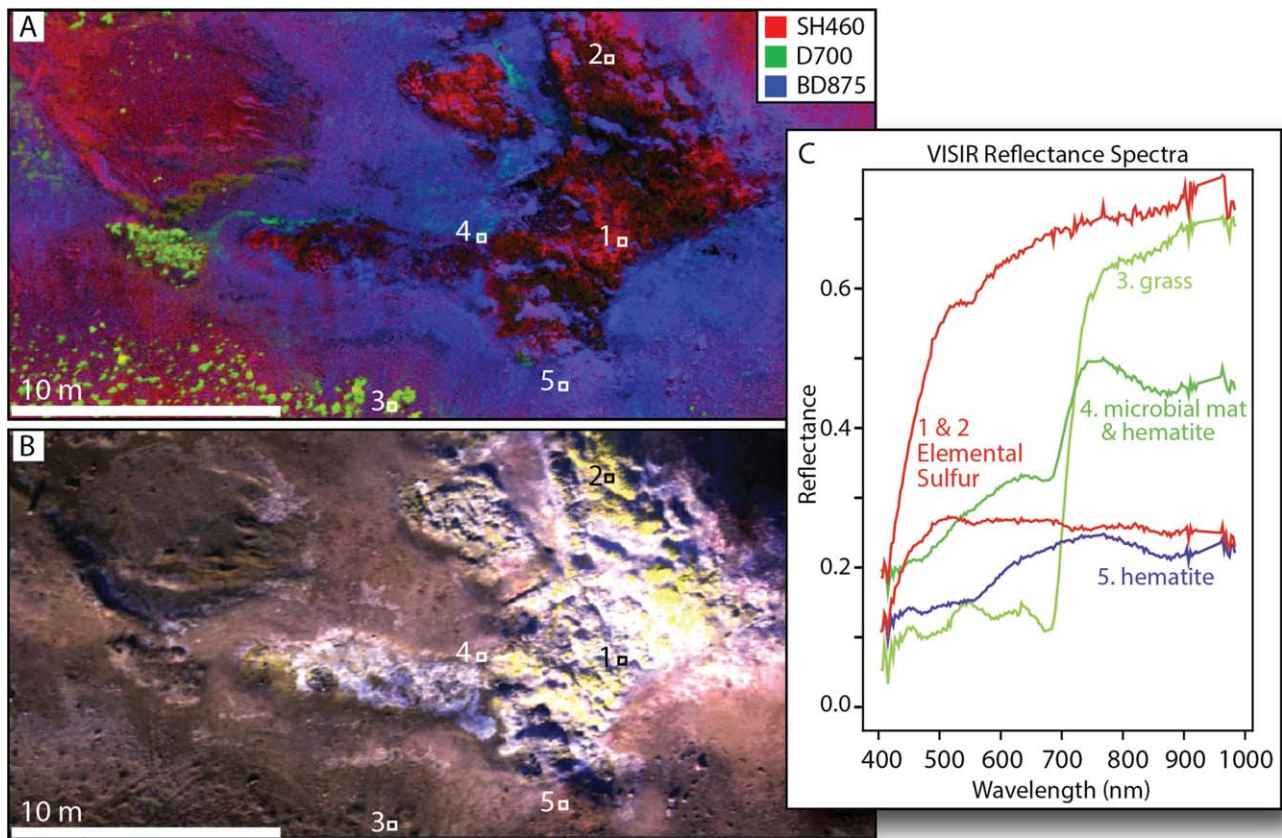
Figure 7. Spectral parameters over fumarole vent near Myvatn, Iceland. (A) Custom parameter combination designed to differentiate elemental sulfur, chlorophyll-bearing materials, and iron oxides. (B) Approximate true color browse product, TRU (R637, R550, R463), of the scene shown in (A). (C) Representative spectra from the locations shown in panels (A) and (B).
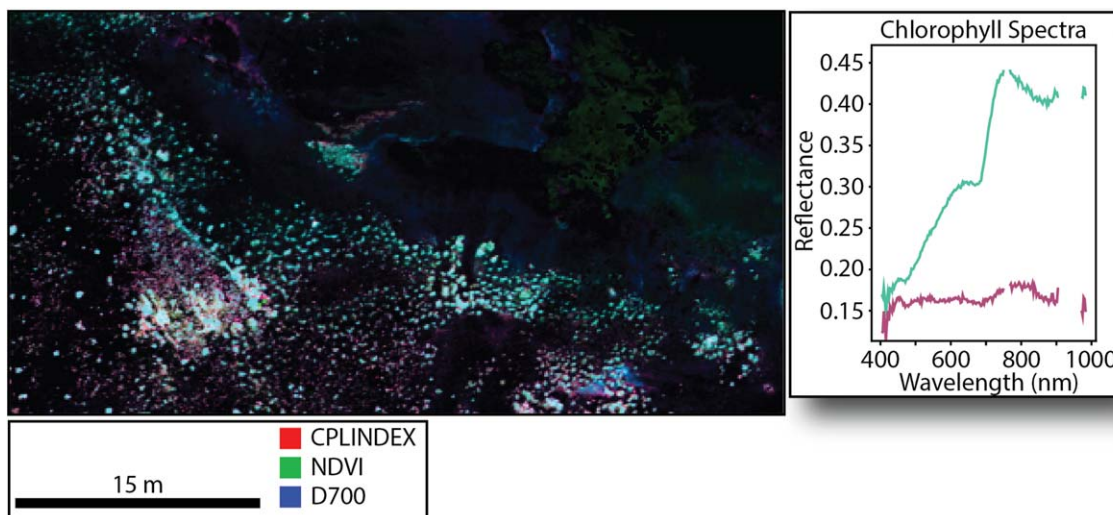
Figure 8. BIO browse product over a fumarole vent near Myvatn, Iceland highlighting different chlorophyll parameters. The NDVI and D700 parameters capture the chlorophyll "red edge" and are better for vegetated areas on land, and the CPLINDEX is better for low signal and water (see Figure 8). The spectral plot shows representative spectra from the seafoam green and burgundy regions of the scene, highlighting chlorophyll with a strong and weak red edge, respectively.

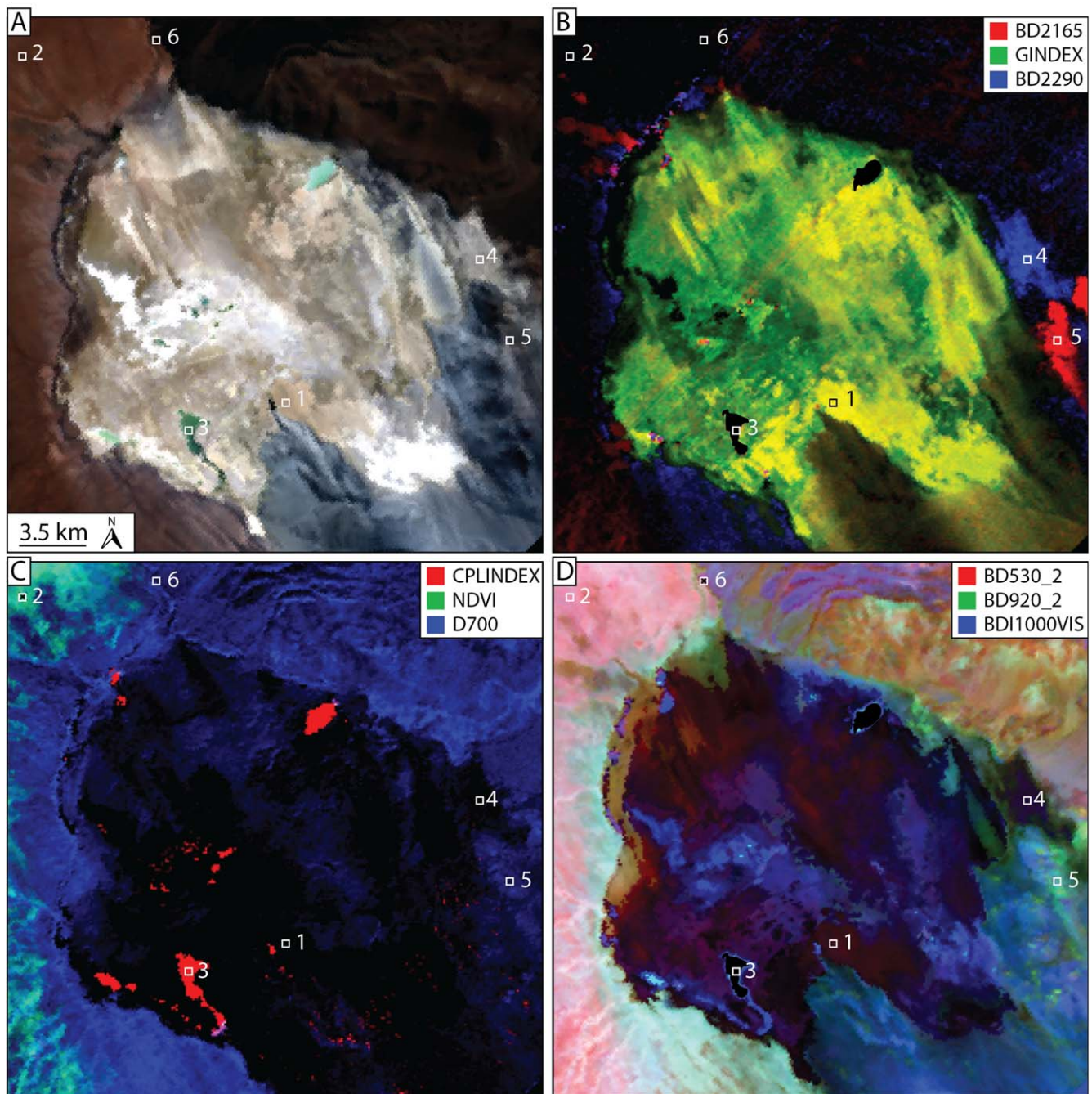### 3.3. Tripod-based Products from Tennessee, USA

Using the Norse Elektrico Optics HySpex Mjolnir VS620 (hereafter HySpex[5]), we collected data from the Section C1, southwest-facing, TN52 roadcut in Tennessee, previously mapped by Stapor Jr.[6] Parameterization of the hyperspectral image cube allows for rapid interpretation of compositional information from the outcrop and for major facies and bedset contacts to be distinguished. The siliciclastic mudstone facies,

---

[5] https://www.hyspex.com/hyspex-products/hyspex-mjolnir/hyspex-mjolnir-vs-620/

[6] https://www.tn.gov/environment/program-areas/tennessee-geological-survey/location-map-tn-52-east-vertical-roadcut-sections-a-h.html

Figure 9. Example HyPyRameter output for an EMIT scene over Salar de Pajonales, Chile. (A) TRU browse product. (B) custom parameter combination to highlight significant minerals within and near Salar de Pajonales (kaolinite = red, gypsum = yellow/green, carbonate = blue). (C) The BIO browse product, which highlights potential pitfalls of the NDVI and the D700 parameters for identifying chlorophyll; these two parameters can be high in the presence of oxides (ROI 2) and can miss chlorophyll in water bodies (ROI 3). (D) FM2 browse product highlighting iron oxides (red/pink, ROI 2), pyroxenes (purple, ROI6), and wet regions of the salar (dark blue to cyan).

comprising illite (BD2210, Figure 6), is readily distinguishable from the crinoidal grainstone and crinoidal pack/wackestone facies, which show signatures of calcium carbonate (BDCARB, Figure 6). Additionally, post-emplacement gypsum efflorescent and goethite alteration are identifiable in the scene. These results demonstrate the potential benefits of incorporating spectral parameter maps for geologic mapping and surveying.

3.4. Drone-based Products from Myvatn, Iceland

The HySpex imager can also be operated in a drone-mounted mode. In this manner, we collected image cubes from a hydrothermal vent near Myvatn, Iceland (U. Basu et al. 2023).

HyPyRameter was used to visualize compositional variation across the scene, with specific focus on iron oxides, elemental sulfur, and chlorophyll (Figure 7). The BD875 parameter tracks the occurrence of hematite, while SH460 highlights elemental sulfur and positive values of D700 indicate chlorophyll. Chlorophyll-bearing microbial mats, observed along the northern rim of the sulfur-rich fumarole vent, are associated with hematite, and appear to follow dispersal pathways downslope away from the vent (Figures 7 and 8). Also demonstrated in this scene are the strengths and weaknesses of three parameters that track chlorophyll: CPLINDEX, NDVI, and D700, which together comprise the BIO browse product. The CPLINDEX is sensitive to chlorophyll
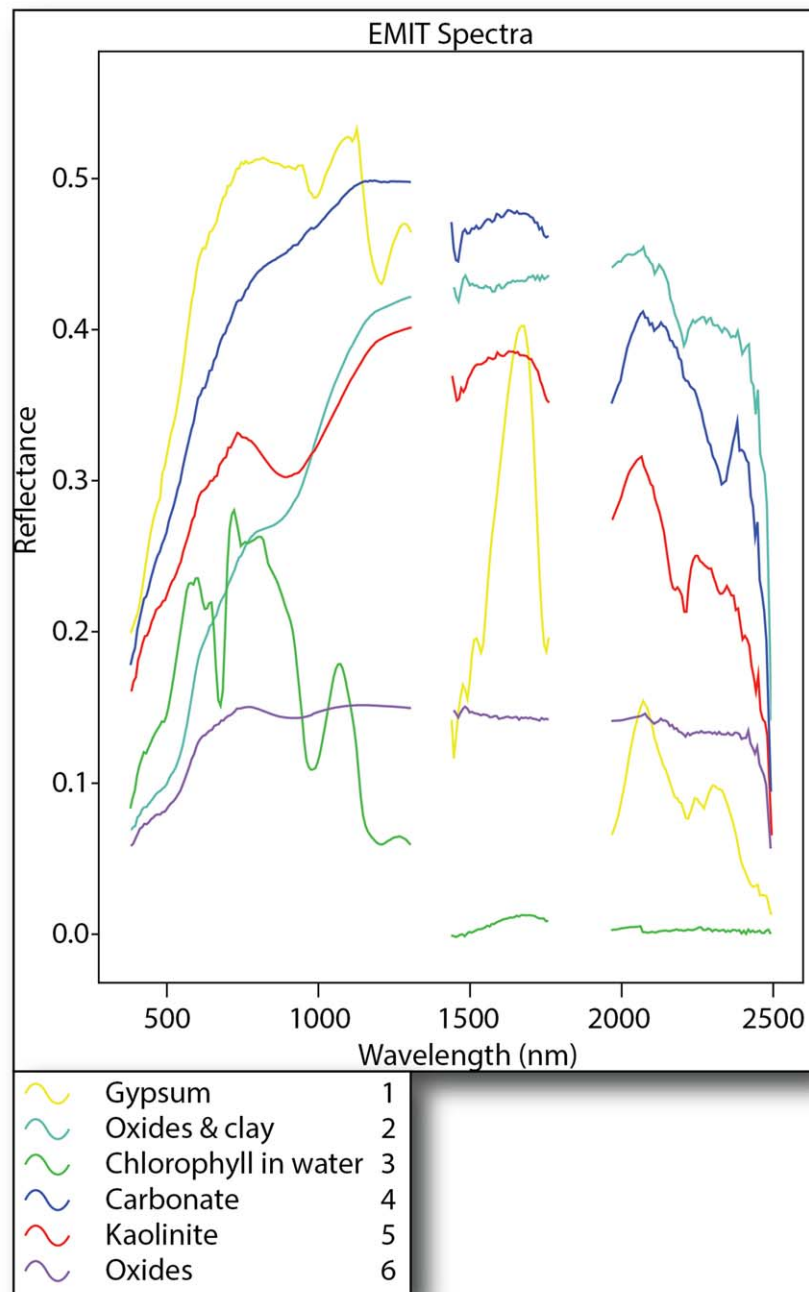
Figure 10. Spectra from ROIs 1–6 in Figure 8.

within a water body (see Figures 9, 10) and chlorophyll in areas with low signal; however, CPLINDEX can yield false positives if the data are noisy. The NDVI and D700 parameters are strongly correlated with one another and more accurately capture the chlorophyll "red edge" than the CPLINDEX but miss chlorophyll signals in low-light and in water.

3.5. Orbit-based Products

Orbit-based platforms are among the most common means by which hyperspectral reflectance data are collected. We produced spectral parameters using HyPyRameter for an Earth Surface Mineral Dust Source Investigation (EMIT; R. O. Green et al. 2023) spectral image cube over the Salar de Pajonales

paleo lake basin in Chile and for the FRT000047A3_07 CRISM scene over Jezero Crater, Mars.

3.5.1. Salar de Pajonales Paleo Lake Basin, Chile

Salar de Pajonales offers mineralogical diversity, which highlights the utility of spectral parameterization. Gypsum is the dominant compositional component of Salar de Pajonales (N. W. Hinman et al. 2022), but lagunas with chlorophyll-bearing microbes, andesitic volcanics, oxides, carbonates, and kaolinite are also present in the scene (M. S. Phillips et al. 2023a). Figure 9 shows different browse product combinations that highlight the spectral diversity at Salar de Pajonales: gypsum, carbonates, and kaolinite are clearly delineated in Figure 9(b) and variations in oxide and pyroxene content in the volcanic terrains surrounding
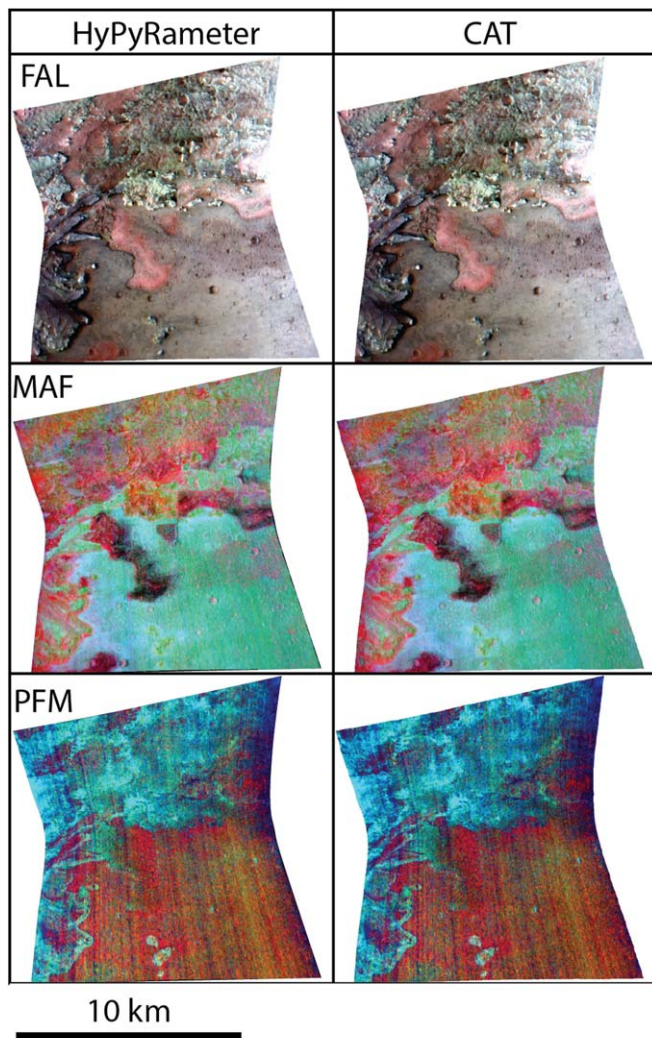
Figure 11. Comparison of HyPyRameter and CRISM Analysis Toolkit (CAT) spectral parameter products. Stretch values for both scenes are set to the same values.

Salar de Pajonales are highlighted with the FM2 browse product in Figure 9(d). The BIO browse product highlights the utility of the CPLINDEX for chlorophyll signatures in water bodies and the potential pitfalls of D700 and NDVI, which in Figure 9(c) highlight oxides rather than chlorophyll and is further evidenced by spectra shown in Figure 10.

3.5.2. Jezero Crater, Mars

FRT000047A3_07 is a well-studied CRISM image over Jezero Crater's western rim and delta, which is the landing site of the Mars 2020 Perseverance rover (K. A. Farley et al. 2020). Figure 11 shows a comparison between HyPyRameter browse products and CRISM Analysis Toolkit (CAT)-derived browse products with the same stretch limits. HyPyRameter was largely based on CRISM spectral parameters, and as such the results from both processing pipelines are nearly identical (typical differences <1e-3, see Figure A2). HyPyRameter offers users the means to extend the application of CRISM-like, and other, spectral parameters to any hyperspectral reflectance data set.

4. Discussion and Conclusions

HyPyRameter was developed to facilitate the interpretation of reflectance spectra acquired as part of the RAVEN simulated

mission operations. The capability of the HyPyRameter tool has since been expanded, and we have shown several examples of its use across a diverse set of hyperspectral data. Spectral parameters are a useful data reduction and visualization technique, and HyPyRameter facilitates the inclusion of this technique in the remote sensing scientist's data-processing workflow. HyPyRameter is a free, open-source tool based in Python, providing access to a wider audience of users than proprietary software, such as ENVI, and flexibility to create custom parameter functions and workflows. Practical applications of HyPyRameter include use for mission operations to make near real-time decisions about hyperspectral data, mineral resource exploration, agricultural monitoring, and geologic mapping. HyPyRameter is developed on GitHub,[7] archived on Zenodo[8] (M. Phillips & C. J. T. Udovicic 2024), and can be installed via Anaconda.[9]

Authorship contribution

M.S.P.: conceptualization, data collection/curation, formal analysis, methodology, software development and repository management, validation, visualization, manuscript original draft and editing. C.T.U.: software development and repository management, validation, manuscript review and editing. J.E.M.: data collection, manuscript review and editing. U.B.: data collection, manuscript review and editing. C.W.H.: data collection, manuscript review and editing, funding acquisition, project administration.

Code Availability

Name: HyPyRameter
Contact: phillipsm@arizona.edu
Hardware requirements: Mac, Windows, Linux
Program language: Python
Software required: Conda
Program size: 46.7 kB
The source codes are available for download at https://github.com/Michael-S-Phillips/HyPyRameter.

Data Availability

The data used to make the figures in this manuscript are available for download at Zenodo, doi:10.5281/zenodo.13786090 (M. Phillips & C. J. T. Udovicic 2024).

---

[7] https://github.com/Michael-S-Phillips/HyPyRameter
[8] https://zenodo.org/records/10801542
[9] https://anaconda.org/michael–s–phillips/hypyrameter

Appendix

Figure A1 illustrates the sensitivity of parameter calculations to the introduction of Gaussian noise to the data. Figure A2 provides a more detailed comparison between parameters generated by HyPyRameter and the CRISM Analysis Toolkit. Table A1 details the parameters available in HyPyRameter, their formulas, and rationales.
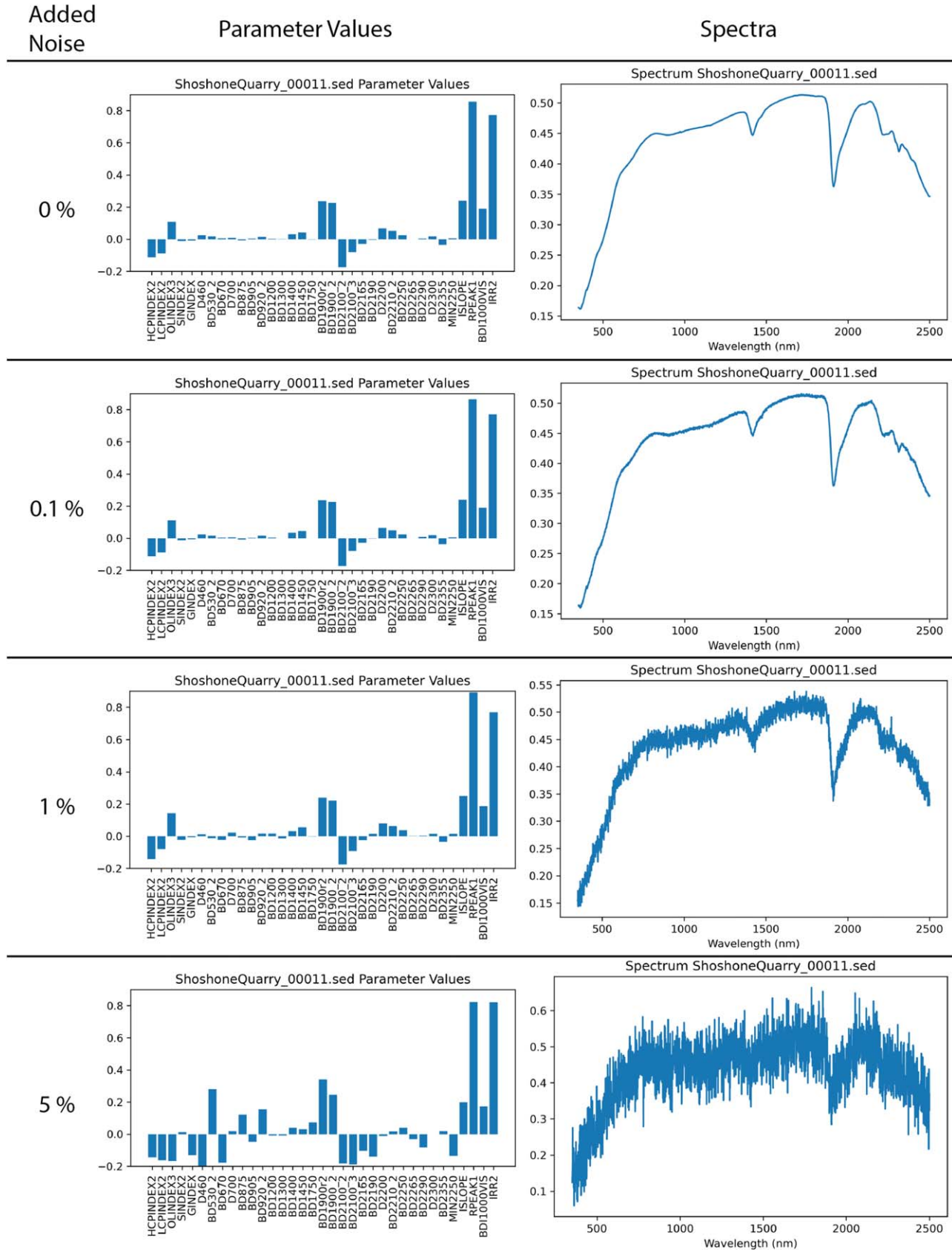
Figure A1. Assessment of spectral parameter response to the addition of stochastic noise at 0.1%, 1%, and 5% levels. Parameter values are largely unaffected at the 1% level (differences max at ∼0.04) but are significantly different at the 5% level.
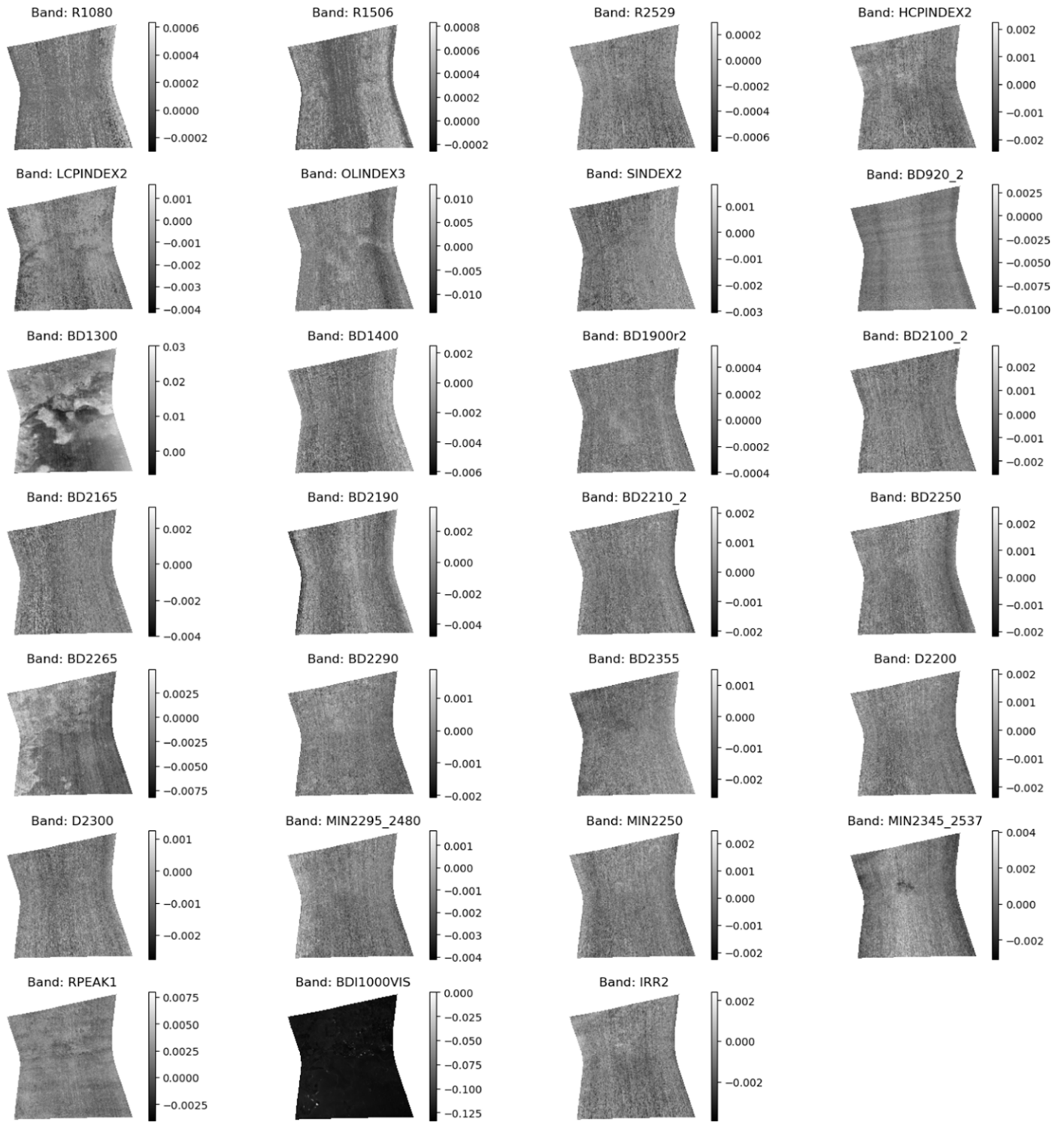
Figure A2. Difference images between HyPyRameter and CAT (CRISM Analysis Toolkit) calculated parameters.

Table A1
Parameters, Formulas, Rationales, and Caveats

Type		Parameter	Formula	Rationale	Caveats
Reflectance	1	R463	R463	Used for TRU browse product	…
	2	R550	R550	Used for TRU browse product	…
	3	R637	R637	Used for TRU browse product	…
	4	R1080	R1080	Used for FAL browse product	…
	5	R1506	R1506	Used for FAL browse product	…
	6	R2529	R2529	Used for FAL browse product	…
Index	7	HCPINDEX2	$(1 - (R2120/Rc2120))^*0.1) + ((1 - (R2140/Rc2140))^*0.1) + ((1 - (R2230/Rc2230))^*0.15) + ((1 - (R2250/Rc2250))^*0.3) + ((1 - (R2430/Rc2430))^*0.2) + ((1 - (R2460/Rc2460))^*0.15$	Pyroxene is strongly +, favors HCP	LCP
	8	LCPINDEX2	$(1 - (R1690/Rc1690))^*0.2) + ((1 - (R1750/Rc1750))^*0.2) + ((1 - (R1810/Rc1810))^*0.3) + ((1 - (R1870/Rc1870))^*0.3$	Pyroxene is strongly +, favors LCP	…
	9	OLINDEX3	$((Rc1210 - R1210)/(abs(Rc1210)))^*0.1) + (((Rc1250 - R1250)/(abs(Rc1250)))^*0.1) + (((Rc1263 - R1263)/(abs(Rc1263)))^*0.2) + (((Rc1276 - R1276)/(abs(Rc1276)))^*0.2) + (((Rc1330 - R1330)/(abs(Rc1330)))^*0.4$	Olivine strongly +	HCP, oxides, Fe-phyllosilicates
	10	SINDEX2	$1 - ((a^*R2120 + b^*R2400)/R2290)$	Hydrated sulfates (mono and poly-hydrated sulfates) will be strongly +	Ices, water, moist soil
	11	GINDEX	MIN(BD(1447), BD(1491), BD(1540))	Gypsum triplet is +	…
	12	CPLINDEX	MIN(BD(630), BD(678))	Chlorophyll in water bodies	Can miss chlorophyll that only presents the "red edge"
Band Depth	13	BD530_2	$1 - (R530/(a^*R440 + b^*R614))$	Hematite, fine-grained yields higher values	…
	14	BD670	$1 - (R670/(a^*R620 + b^*R745))$	Ferric oxides and chlorophyll	…
	15	BD875	$1 - (R875/(a^*R747 + b^*R980))$	Ferric oxides (hematite)	…
	16	BD905	$1 - (R750/(a^*R905 + b^*R1300))$	Ferric oxides (goethite), LCP, liquid water	…
	17	BD920_2	$1 - (R807/(a^*R920 + b^*R984))$	Ferric minerals and LCP	…
	18	BD1200	$1 - (R1200/(a^*R1115 + b^*R1260))$	Liquid water, vegetation, hydrated minerals (gypsum)	…
	19	BD1300	$1 - (R1320/(a^*R1260 + b^*R1750))$	Plagioclase with Fe2+	Olivine is +
	20	BD1400	$1 - (R1395/(a^*R1330 + b^*R1467))$	Liquid water, vegetation, hydrated/hydroxalted minerals (e.g., gypsum)	…
	21	BD1450	$1 - (R1450/(a^*R1340 + b^*R1535))$		…

Type		Parameter	Formula	Rationale	Caveats
				Liquid water, vegetation, some hydrated minerals	
	22	BD1750	$1 - (R1750/(a^*R1688 + b^*R1820))$	Gypsum, alunite	…
	23	BD1900_2	$1 - (R1930/(a^*R1850 + b^*R2067))$	Bound molecular water	…
	24	BD1900r2	$1 - ((R1908/Rc1908 + R1914/Rc1914 + R1921/Rc1921 + R1928/Rc1928 + R1934/Rc1934 + R1941/Rc1941)/(R1862/Rc1862 + R1869/Rc1869 + R1875/Rc1875 + R2112/Rc2112 + R2120/Rc2120 + R2126/Rc2126))$	Bound molecular water	…
	25	BD2100_2	$1 - (R2132/(a^*R1930 + b^*R2250))$	Water in monohydrated sulfates	…
	26	BD2100_3	$1 - (R2100/(a^*R2016 + b^*R2200))$	Hydrated silica, Al-smectites	monohydrated sulfates
	27	BD2165	$1 - (R2165/(a^*R2120 + b^*R2230))$	Pyrophyllite, Kaolinite group	Gypsum
	28	BD2190	$1 - (R2185/(a^*R2120 + b^*R2250))$	Beidellite, allophane, imogolite	kaolinite group
	29	BD2210_2	$1 - (R2210/(a^*R2165 + b^*R2240))$	Al-OH minerals	Gypsum, alunite
	30	BD2250	$1 - (R2245/(a^*R2120 + b^*R2340))$	Hydrated silica, Al-OH minerals	…
	31	BD2265	$1 - (R2265/(a^*R2120 + b^*R2340))$	Jarosite, gibbsite, acid-leached nontronite	…
	32	BD2290	$1 - (R2290/(a^*R2250 + b^*R2350))$	Mg,Fe-OH minerals, carbonate	…
	33	BD2355	$1 - (R2355/(a^*R2300 + b^*R2450))$	Chlorite, prehnite, pumpellyite, carbonate, serpentine	…
	34	BD2600	$1 - (R2600/(a^*R2530 + b^*R2630))$	Carbonates	water vapor
	35	BDCARB	$1 - (((((R2320 + R2330)^*0.5)/(b_1{}^*R2230 + a_1{}^*R2390))^*(((R2520 + R2530)^*0.5)/(b_2{}^*R2390 + a_2{}^*R2600)))^.0.5)$	Carbonates	Hydroxylated silicate phases
Band Area	36	BA1200	Integral of a cubic spline fit to the continuum-removed spectrum between 1115 and 1260 nm	Liquid water, vegetation, hydrated minerals (gypsum)	…
	37	BA1450	Integral of a cubic spline fit to the continuum-removed spectrum between 1340 and 1535 nm	Liquid water, vegetation, some hydrated minerals	…
	38	BA1900	Integral of a cubic spline fit to the continuum-removed spectrum between 1850 and 2067 nm	Bound molecular water	…
Shoulder	39	SH460	$1 - ((a^*R420 + b^*R520)/R460)$	Elemental sulfur	…
	40	D700	$1 - (((R690/Rc690) + (R710/Rc710) + (R720/Rc720))/((R740/Rc740) + (R760/Rc760) + (R770/Rc770)))$	Chlorophyll	Some oxides
	41	D2200	$1 - (((R2210/Rc2210) + (R2230/Rc2230))/(2^*(R2165/Rc2165)))$	Al-OH minerals	Chlorite, prehnite
	42	D2300	$1 - (((R2290/Rc2290) + (R2320/Rc2320) + (R2330/Rc2330))/((R2120/Rc2120) + (R2170/Rc2170) + (R2210/Rc2210)))$	Hydroxylated Fe,Mg silicates	Carbonate

Table A1
(Continued)

Type		Parameter	Formula	Rationale	Caveats
Minimum	43	MIN2295_2480	MIN(BD(2295), BD(2480))	Mg carbonates (both overtones must be present)	Hydroxylated silicate + zeolite mixtures
	44	MIN2250	MIN(BD(2210), BD(2265))	Hydrated silica (opal)	⋯
	45	MIN2345_2537	MIN(BD(2345), BD(2265))	Ca/Fe carbonates (both overtones must be present)	Prehnite, serpentine, hydroxylated silicate + zeolite mixtures
Peak	46	RPEAK1	Wavelength where first derivative = 0 of the fifth-order polynomial fit to reflectance values between 442 and 989 nm	Used for BDI1000VIS, tracks dust on Mars	⋯
Integrated Band Depth	47	BDI1000VIS	Integral of (1 − reflectance values between 442 and 989 nm normalized to the reflectance value at the RPEAK1 wavelength)	Olivine, pyroxene, Fe-bearing class	Some oxides, Fe-bearing phyllosilicates, liquid water
Slope	48	SLOPE1815_2530	$1000 \, ^* \, (R1815 - R2530)/(W2530 - W1815)$	(ISLOPE1 in CRISM parameters) ferric coating on dark rock	⋯
Band Ratio	49	BR800	R800/R997	(IRR1 in CRISM parameters) Ice clouds and dust on Mars	⋯
	50	BR2530	R2530/R2210	(IRR2 in CRISM parameters) Ice clouds and dust on Mars	⋯
	51	BR3500	R3500/R3390	(IRR3 in CRISM parameters) Ice clouds and dust on Mars	⋯
Normalized Difference Indices	52	NDVI	(R833 − R665)/(R833 + R665)	Normalized Difference Vegetation Index, tracks vegetation on land	⋯
	53	NDWI	(R560 − R833)/(R560 + R833)	Normalized Difference Water Index, tracks water bodies	⋯
	54	NDMI	(R833 − R1670)/(R833 + R1670)	Normalized Difference Moisture Index, tracks moisture in vegetation	⋯

Note. Compare with Table 2 from C. E. Viviano et al. (2014).

ORCID iDs

Christian Tai Udovicic ● https://orcid.org/0000-0001-9972-1534
Christopher W. Hamilton ● https://orcid.org/0000-0001-9731-517X

References

Adams, J. B. 1974, Visible and Near-infrared Diffuse Reflectance Spectra of Pyroxenes as Applied to Remote Sensing of Solid Objects in the Solar System, JGR, 79, 4829

Adams, J. B., & Filice, A. L. 1967, Spectral Reflectance 0.4 to 2.0 microns of Silicate Rock Powders, JGR, 72, 5705

Basu, U., Schroedl, P., Phillips, M., et al. 2023, Correlating Aerial and Ground-based Hyperspectral Data with Microbial Composition and Diversity in a Mars Analog Hydrothermal System in Iceland, LPSC, 54, 1840

Burns, R. G. 1993, Mineralogical Applications of Crystal Field Theory (Cambridge: Cambridge Univ. Press)

Carr, B. B., Varnam, M., Hadland, N., et al. 2024, Evaluating the Use of Unoccupied Aircraft Systems (UASs) for Planetary Exploration in Mars Analog Terrain, PSJ, 5, 231

Clark, R. N., King, T. V. V., Klejwa, M., Swayze, G. A., & Vergo, N. 1990, High Spectral Resolution Reflectance Spectroscopy of Minerals, JGR, 95, 12653

Clark, R. N., & Roush, T. L. 1984, Reflectance Spectroscopy: Quantitative Analysis Techniques for Remote Sensing Applications, JGR, 89, 6329

Clark, R. N., Swayze, G. A., Livo, K. E., et al. 2003, Imaging Spectroscopy: Earth and Planetary Remote Sensing with the USGS Tetracorder and Expert Systems, JGRE, 108, 5131

Farley, K. A., Williford, K. H., Stack, K. M., et al. 2020, Mars 2020 Mission Overview, SSRv, 216, 142

Green, R. O., Mahowald, N., Thompson, D. R., et al. 2023, Performance and Early Results from the Earth Surface Mineral Dust Source Investigation (EMIT) Imaging Spectroscopy Mission, in 2023 IEEE Aerospace Conf. (Piscataway, NJ: IEEE), 1

Gwizd, S., Stack, K. M., Francis, R., et al. 2024, Comparing Rover and Helicopter Planetary Mission Architectures in a Mars Analog Setting in Iceland, PSJ, 5, 172

Hamilton, C., Voight, J. R. C., Carr, B. B., et al. 2024, PSJ, submitted

Hinman, N. W., Hofmann, M. H., Warren-Rhodes, K., et al. 2022, Surface Morphologies in a Mars-analog Ca-Sulfate Salar, High Andes, Northern Chile, FrASS, 8, 797591

Kokaly, R., Clark, R. N., Swayze, G. A., et al. 2017, USGS Spectral Library Version 7 Data, doi:10.5066/F7RR1WDJ

Macenka, S. A., & Chrisp, M. P. 1987, Airborne Visible/Infrared Imaging Spectrometer (Aviris) Spectrometer Design And Performance, Proc. SPIE, 834, 32

Moersch, J., Mondro, C., Leight, C. J., & Phillips, M. 2020, A New Community Resource for Terrestrial Analog Field Research: A Visible to Shortwave Infrared (400–2500 nm) Drone- and Ground-based Hyperspectral Imager for High Resolution Compositional Mapping, LPSC, 51, 1865

Murchie, S., Arvidson, R., Bedini, P., et al. 2007, Compact Reconnaissance Imaging Spectrometer for Mars (CRISM) on Mars Reconnaissance Orbiter (MRO), JGRE, 112, E05S03

Pedersen, G. B. M., Höskuldsson, A., Dürig, T., et al. 2017, Lava Field Evolution and Emplacement Dynamics of the 2014–2015 Basaltic Fissure Eruption at Holuhraun, Iceland, JVGR, 340, 155

Pelkey, S. M., Mustard, J. F., Murchie, S., et al. 2007, CRISM Multispectral Summary Products: Parameterizing Mineral Diversity on Mars from Reflectance, JGRE, 112, E08S14

Phillips, M. S., McInenly, M., Hofmann, M. H., et al. 2023a, Salt Constructs in Paleo-Lake Basins as High-priority Astrobiology Targets, RemS, 15, 314

Phillips, M. S., Murchie, S. L., Seelos, F. P., et al. 2023b, A First look at CRISM Hyperspectral Mapping Mosaicked Data: Results from Mawrth Vallis, Icar, 419, 115712

Phillips, M., & Udovicic, C. J. T. 2024, Michael-S-Phillips/HyPyRameter: HyPyRameter v0.2.0, Zenodo, doi:10.5281/zenodo.10801542

Stein, N. T., Grotzinger, J. P., Quinn, D. P., et al. 2023, Geomorphic and Environmental Controls on Microbial Mat Fabrics on Little Ambergris Cay, Turks and Caicos Islands, Sedim, 70, 1915

Van Gorp, B., Mouroulis, P., Blaney, D. L., et al. 2014, Ultra-compact Imaging Spectrometer for Remote, In Situ, and Microscopic Planetary Mineralogy, JARS, 8, 084988

Viviano, C. E., Seelos, F. P., Murchie, S. L., et al. 2014, Revised CRISM Spectral Parameters and Summary Products based on the Currently Detected Mineral Diversity on Mars, JGRE, 119, 1403

Voigt, J. R. C., Hamilton, C. W., Scheidt, S. P., et al. 2021, Geomorphological Characterization of the 2014–2015 Holuhraun Lava Flow-field in Iceland, JVGR, 419, 107278